Fermi National Accelerator Laboratory

FERMILAB-Conf-82/97-EXP
7190.497

CHARGED HYPERON PRODUCTION BY 400 GEV/c PROTONS

L. J. Teig, E. W. Anderson, C. Ankenbrandt, J. P. Berge, A. Breakstone, A. E. Brenner, J. Butler, T. R. Cardello, P. S. Cooper, K. Doroba, J. Elias, J. Lach, P. Laurikainen, J. MacLachlan, J. P. Marriner, E. McCliment, E. I. Rosenberg, J. L. Thron, Y. W. Wah

Fermi National Accelerator Laboratory, University of Iowa, Iowa State University, and Yale University

December 1982

*Submitted to the 5th International Symposium on High Energy Spin Physics, Brookhaven National Laboratory, September 16-22, 1982

CHARGED HYPERON PRODUCTION BY 400 GEV/c PROTONS

L. J. Teig, E. W. Anderson, C. Ankenbrandt, J. P. Berge,
A. Breakstone, A. E. Brenner, J. Butler, T. R. Cardello,
P. S. Cooper, K. Doroba, J. Elias, J. Lach, P. Laurikainen,
J. MacLachlan, J. P. Marriner, E. McCliment, E. I. Rosenberg,
J. L. Thron, Y. W. Wah
Fermilab, Univ. of Iowa, Iowa State Univ. and Yale Univ.

We report preliminary results from Fermilab Experiment E-497 on the x and p_t dependence of charged hyperon and anti-hyperon production by 400 GeV/c protons on a Cu target.

This paper on charged hyperon production is one of three reports at this conference presenting results of E-497. The other papers report on Σ^+ and Σ^- magnetic moments[1] and polarizations[2]. Figure 1 of reference 2 shows the apparatus which, for the data reported in this paper, differed only in that the front lead glass array was removed, and that for the 100 GeV/c data, the decay region length was 12 m rather than the 20 m length used at higher momenta. The second lead glass array, though in place, was not used in this analysis.

The dump magnet is 7 m long, with the magnetic field integral adjustable up to 25 T-m, allowing us to select a secondary beam momentum up to 360 GeV/c. The solid angle acceptance of the channel is 0.64 μsr and the momentum acceptance is ±7% at the base of the distribution. The channel bend angle is 20 mrad. The 400 GeV/c proton beam coming into the hyperon magnet can be steered, allowing us to target the protons with angles up to 7 mrad with respect to the secondary beam. The steering can be done either vertically or horizontally, though not both at the same time. The data presented here include both types of steering. The copper target, starting 6 cm inside the dump magnet, is 14.8 cm long with a cross section of 2 mm x 2 mm. The proton beam has a 1 mm diameter at the target.

A system of four proportional wire chambers with effective 203 μm wire spacing is located in the 3 meters immediately downstream of the dump magnet. This system gives us 60 μm(σ) position resolution and 30 μrad(σ) angular resolution, allowing us to reconstruct the secondary beam particle momentum with a 0.7% σ. The decay region begins downstream of the last PWC and includes the gap in the muon spoiler. The length of the decay region, as previously mentioned, was varied depending on the secondary beam momentum, by moving the drift chamber spectrometer.

The drift chamber spectrometer which follows the decay region consists of two magnets with a p_t kick of ~.8 GeV/c each, and drift chambers, three in front of the first magnet, three between the two magnets, and one downstream of the second magnet. This last drift chamber is used to measure the momentum of secondary beam particles which didn't decay and proton momenta from the $\Sigma^+ \to p\pi^0$ decay and the $\Xi^- \to \pi^- \Lambda \to p\pi^-$ decay. The π^- from the $\Sigma^- \to n\pi^-$, $\Xi^- \to \Lambda\pi^-$ and $\Lambda \to p\pi^-$ and the π^+ from $\Sigma^+ \to n\pi^+$ have too low momenta to hit this last drift chamber. This system then gives 200 μm position resolution, 100 μrad angular resolution, and approximately .7% momentum resolution for decay pions

and 50 μrad angular resolution and 1.5% momentum resolution for decay protons and beam particles. The drift chamber spectrometer has 100% geometrical acceptance for hyperon decays within the decay fiducial volume. The decay angle resolution of 100 μrad is limited by the drift chamber resolution, and this angular resolution limits our mass resolution for O-C fits to $\Sigma \to n\pi$ and $\Xi \to \Lambda\pi$ with the Λ decaying into neutral particles. The Σ^- mass resolution is 3.6 MeV (σ) at a secondary beam momentum of 100 GeV/c, and 4.6 MeV at 260 GeV/c. The Ξ^- mass resolution is 3.2 MeV at 100 GeV/c and 3.8 MeV at 250 GeV/c, and is better than the Σ^- mass resolution due to the smaller p_t in the decay.

The final piece of apparatus was a neutron calorimeter three absorption lengths long. With the minimum energy requirement in the trigger the neutron calorimeter was ~80% efficient as a neutron detector. The calorimeter was preceded by a scintillation counter used as a charged particle veto.

We typically ran with a 10^4 particle per second beam flux. This flux, depending on the kinematic conditions, on the average required a flux of 2×10^{10} protons per second on the production target.

Charged hyperon decays give two different track topologies in our apparatus. The decays $\Sigma \to n\pi$, $\Xi \to \Lambda\pi$ and $\Omega \to \Lambda K$ with the Λ decaying neutrally give one charged track through the apparatus along with large energy deposition in the neutron calorimeter. If the Λ in the above decays itself decays through its charged mode, we get three charged tracks through the drift chamber spectrometer. The two topologies had separate triggers and are analyzed separately.

First we discuss the results of the one-track topology analysis. The error bars represent purely statistical errors, unless otherwise indicated. Our systematic errors are due mainly to our use of the cross section parameterizations of other experiments. The single track reconstruction efficiency is higher than 99% both for beam tracks and for hyperons decaying in the fiducial volume. In this analysis, only the $n\pi^+$ decay mode is used to determine the Σ^+ flux. The number of $n\pi^+$ decays is divided by the branching ratio[4] to find the number of Σ^+ in the beam.

Figure 1 represents a plot of P_t versus $P_{\parallel}$ in the parent center of mass for decay events in one 260 GeV/c data run, assuming the decay is $\Sigma^- \to n\pi^-$. Except for the fact that the two scales are different, we see a circle due to decays ($P_t' = \sqrt{P_t^2 + P_{\parallel}^2}$ is a constant) and a second band with fewer events, clearly separated from the first, due to Ξ^- one-track decays. The only cuts here are a fiducial cut, a minimum P_t cut of .02 GeV/c, and a target reconstruction cut. The P_t cut allows us to reconstruct the vertex with greater accuracy.

Figure 2 represents the mass distribution of Σ^- candidates using the same cuts above. We fit the distribution assuming a gaussian peak with linear background, and find that within four standard deviations of the peak, the signal to background is 18 to 1. The number of sigmas found to lie in the gaussian peak is then corrected by Monte Carlo methods to account for effects of the above cuts and for events that decay downstream of the fiducial volume in order to find the flux at the front of the fiducial volume.

Figures 3a and 3b give the corrected hyperon fluxes as a fraction of the total secondary beam flux ten meters downstream of the target, i.e., three meters downstream of the dump magnet. In these figures, the vertical bars represent the variation in the beam fraction due to targeting angle changes at the indicated momentum settings rather than statistical errors. These high rates show why this beam is such a nice facility to study hyperon properties.

We now again use a Monte Carlo to calculate, starting with the number of events at the front of the fiducial volume, what the number of hyperons leaving the production target must have been. Also, we find the number of events that went through our apparatus without decaying, subtract the number of undecayed hyperons, and then, using the data of Bourquin et al.[3], find the fraction of beam particles which are pions and thus calculate the pion flux through our apparatus. We correct the pion and hyperon fluxes for target reabsorption[5] and then take the ratios of the corrected hyperon flux to the corrected pion flux. All the following results are hyperon to pion flux ratios. We quote ratios since we don't know the absolute acceptance of our channel or the absolute primary proton flux well enough to determine the absolute secondary particle production cross sections. We then calculate the absolute cross sections by using other measurements of the absolute pion production cross section, for instance, in Bourquin et al.[3]

Figure 4 shows the corrected Σ^+ to π^+ production ratio data at the different kinematic points. x is Feynman x, and for us, is effectively the secondary beam momentum divided by 400 GeV/c. p_t is the product of the secondary beam momentum and the hyperon production angle determined by the proton beam steering. The straight lines are fits to the data of the form $A \exp(Bp_t)$ where A and B are constants determined from the fit. We have similar graphs for the other hyperons which we don't show here due to space considerations.

The variation of the constants B with x for the different hyperons is shown in figures 5a-d. We also have one set of kinematic points for the $\bar{\Xi}$ all at x = .25, which fit the form $(.012\pm.004) \exp (.1\pm.6)p_t$ for the $\bar{\Xi}$ to π^+ production ratio. The p_t variation with x is similar to that seen in D. Brick et al.[6]

Next we fit the constants A at the different x values to the form $A(x) = C(1-x)^{n_{ratio}}$ for the different particles. The results are shown in figures 6a and 6b, where we again plot the ratio of hyperon to pion fluxes, now extrapolated to $p_t = 0$. We now add to the n_{ratio} found in the fit, the value of n for pions given in Bourquin et al.[4] to find the absolute n for the particle in the production cross section.

We find the values shown in the table below

Particle	n
Σ^-	.48±.17
Ξ^-	2.6±.2
Σ^+	.72±.34
$\bar{\Sigma}^-$	2.3±.6

The Σ^-, Ξ^- and Σ^+ production cross sections have been measured previously by Bourquin et al.[3] at 200 and 210 GeV/c primary proton momentum. Our fits agree with their data points, showing scaling behavior.

We have just begun to analyze three-track events. On one 250 GeV run, we find a Ξ^- mass peak with a standard deviation of 7 MeV/c^2 using the $\Lambda \rightarrow p\pi^-$ decay mode. We now make a cut to eliminate all events which satisfy the hypothesis of $\Xi^- \rightarrow \Lambda \pi^-$, and try instead the hypothesis $\Omega^- \rightarrow \Lambda K^-$. We find the mass distribution shown in figure 7. We see a clear signal above the background at the Ω^- mass. The number of Ω^- in this peak, after Monte Carlo corrections for decay lifetime, reconstruction efficiency and acceptance, agrees to within a factor of two with a number found by scaling the Ω flux of Bourquin et al.[3] to our energies.

In conclusion, we have measured the Σ^-, Σ^+, Ξ^-, $\overline{\Sigma^-}$, and $\overline{\Xi^-}$ fluxes in the FNAL charged hyperon beam, and the x and p_t dependence of these particles' production cross section using 400 GeV/c protons on a Cu target. We will soon have more results on the Ω^- flux.

REFERENCES

1. J. P. Marriner et al., proceedings of this conference.
2. P. S. Cooper et al., proceedings of this conference.
3. M. Bourquin et al., Nuclear Physics B 153, 13-38, (1979).
   M. Bourquin et al., Zeitschrift fur Physik C, 275-283 (1980).
4. Review of Particle Properties, Rev. Mod. Phys. 52,#2,Pt.II (1980).
5. This includes effects due to inelastic and elastic scattering in the copper target. References are: A. E. Brenner, Proceedings, Seoul Symposium, Elementary Particles, p. 87 (1978), A. Schiz et al., Phys. Rev. D 24, 26 (1981), D. S. Ayres et al., Phys. Rev. D 15, 3105 (1977), Rev. Mod. Phys. 52, S1 (1980).
6. D. Brick et al., Phys. Rev. D 20, 2123 (1979).

FIGURE CAPTIONS

Figure 1. P_t vs. $P_{\parallel}$ in the C of M system of the decaying particle assuming the decay is $\Sigma^- \rightarrow n\pi^-$.

Figure 2. The Σ^- mass distribution for a 250 GeV/c run.

Figure 3a and b. Particle ratios in negative and positive beam at a location 7 meters downstream of the target.

Figure 4. Σ^+/π^+ production ratios, with fits for the p_t dependence of the form $R=A \exp(Bp_t)$.

Figures 5a-d. Graphs of the B values as a function of Feynman x.

Figure 6a and b. The hyperon to pion production ratios extrapolated to $p_t=0$, and fit with the form $R = C(1-x)^n$ ratio The Σ^- point at $1-x=.1$ is not used in the fit.

Figure 7. Ω^- mass distribution.

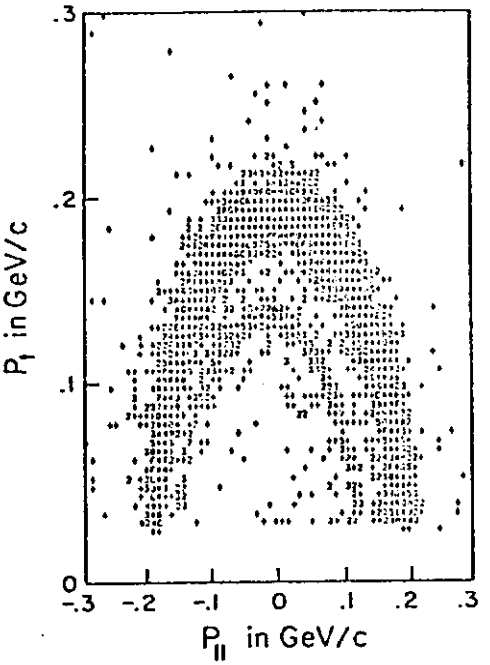

Figure 1

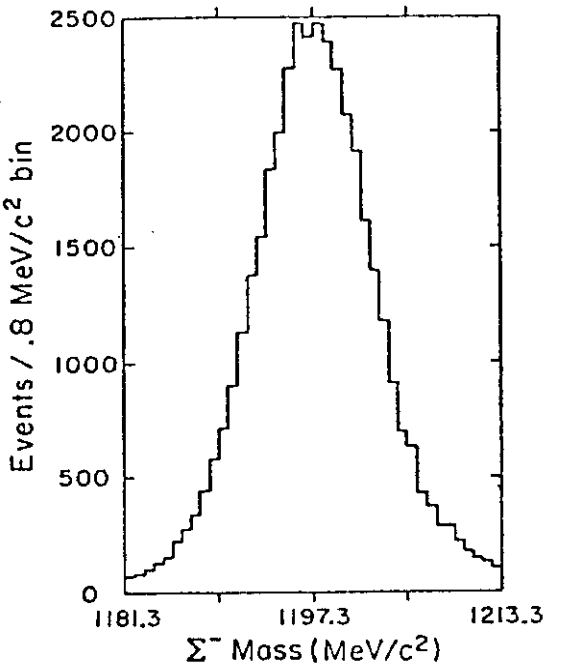

Figure 2

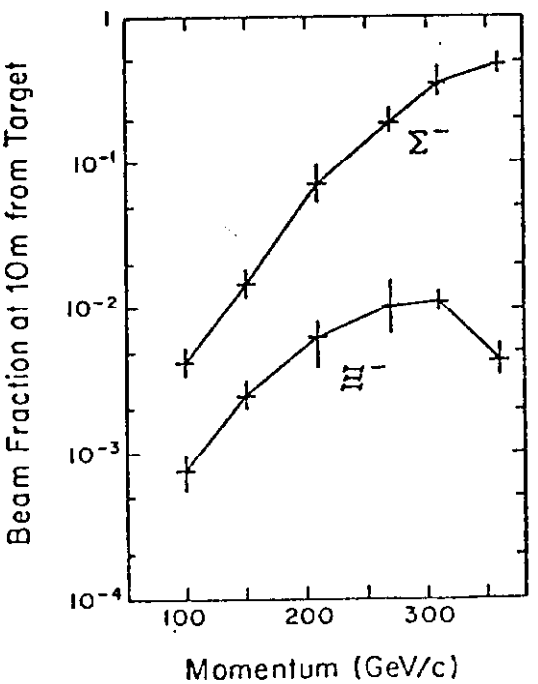

Figure 3a

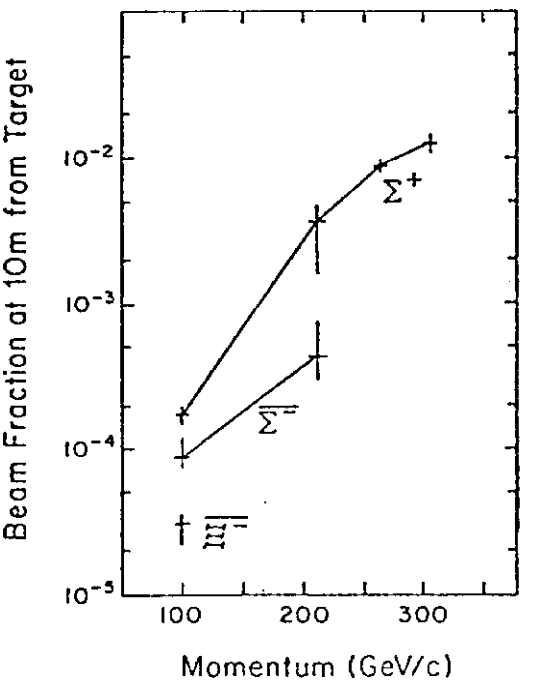

Figure 3b

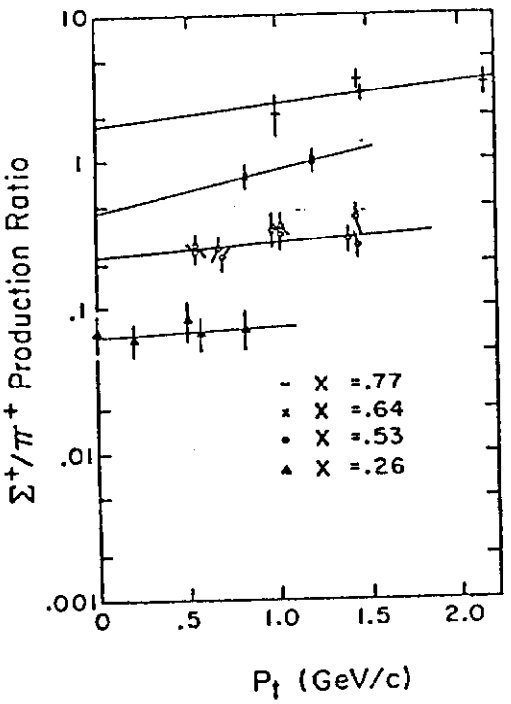

Figure 4

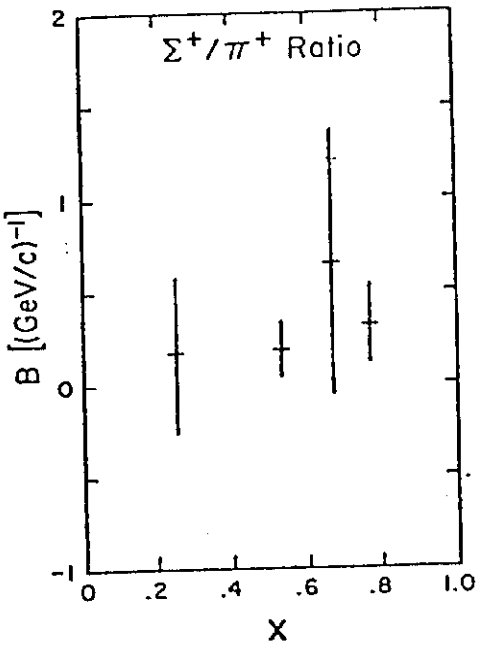

Figure 5a

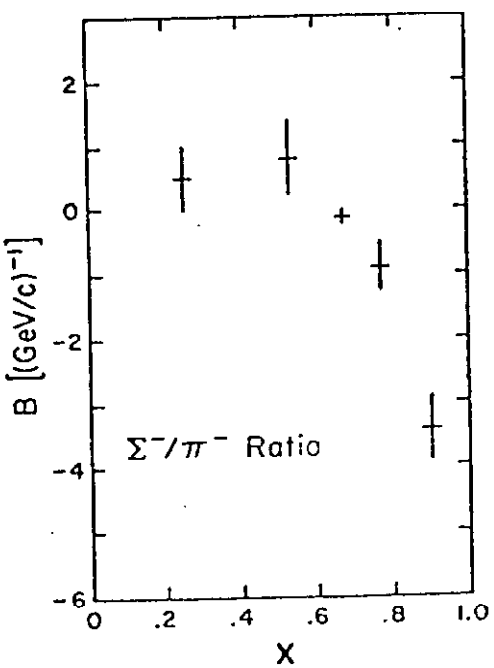

Figure 5b

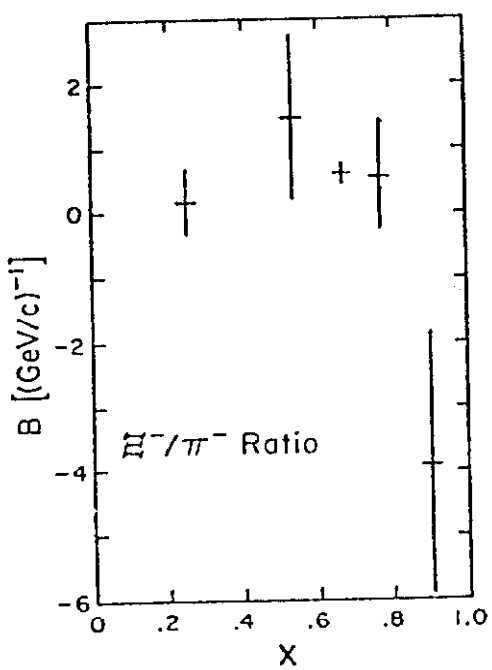

Figure 5c

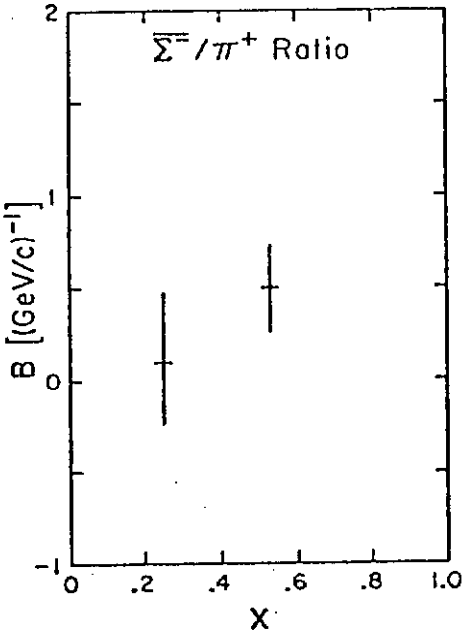

Figure 5d

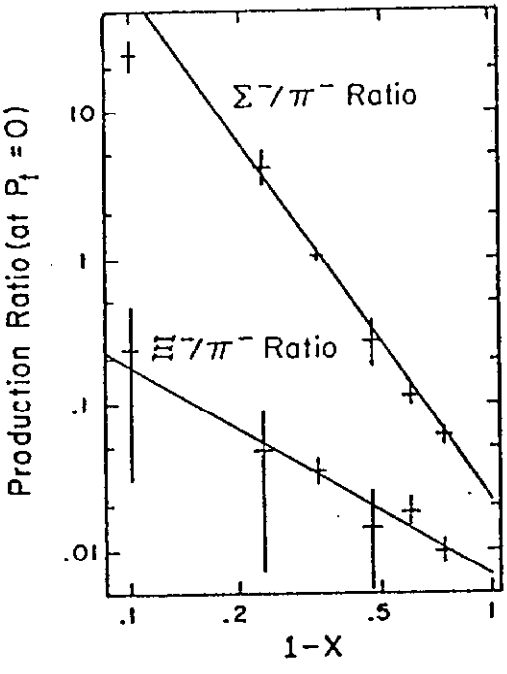

Figure 6a

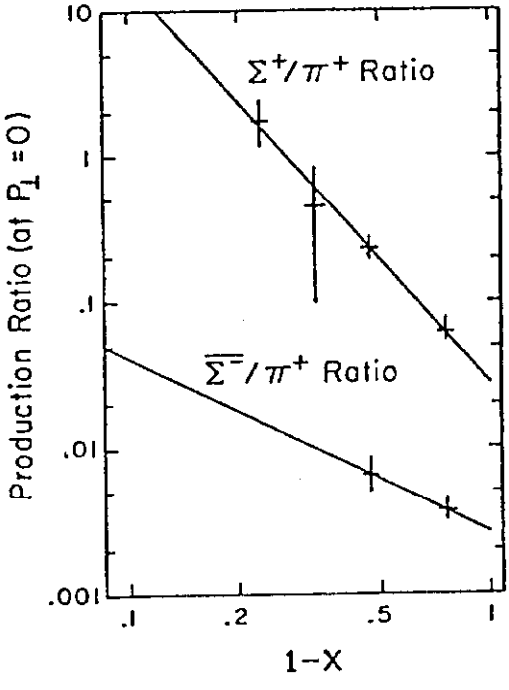

Figure 6b

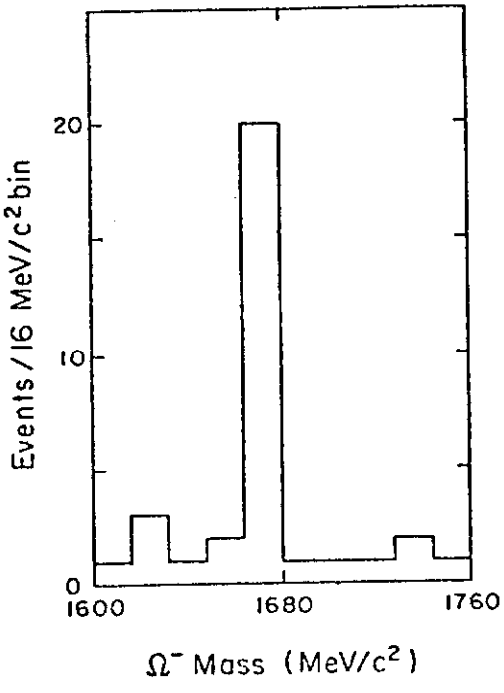

Figure 7